

The **next generation** GBCA  
from Guerbet is here

Explore new possibilities >

Guerbet | 

© Guerbet 2024 GUOB220151-A

# AJNR

## **Diffusion-Weighted MR Imaging of Ameloblastomas and Keratocystic Odontogenic Tumors: Differentiation by Apparent Diffusion Coefficients of Cystic Lesions**

This information is current as  
of July 20, 2024.

M. Sumi, Y. Ichikawa, I. Katayama, S. Tashiro and T.  
Nakamura

*AJNR Am J Neuroradiol* 2008, 29 (10) 1897-1901

doi: <https://doi.org/10.3174/ajnr.A1266>

<http://www.ajnr.org/content/29/10/1897>

ORIGINAL  
RESEARCH

M. Sumi  
Y. Ichikawa  
I. Katayama  
S. Tashiro  
T. Nakamura

# Diffusion-Weighted MR Imaging of Ameloblastomas and Keratocystic Odontogenic Tumors: Differentiation by Apparent Diffusion Coefficients of Cystic Lesions

**BACKGROUND AND PURPOSE:** Ameloblastomas and keratocystic odontogenic tumors are major aggressive odontogenic tumors in the maxillomandibular regions, but the differentiation between these 2 tumors is frequently ineffective based on only conventional CT and MR imaging findings. Here, we evaluated diffusion-weighted MR imaging for the differentiation of these 2 odontogenic tumors.

**MATERIALS AND METHODS:** We prospectively studied 9 patients with ameloblastoma and 7 patients with keratocystic odontogenic tumor using diffusion-weighted MR imaging. Apparent diffusion coefficients (ADCs) of the nonenhancing and solid lesions in these tumors were determined with use of 2 b factors (500 and 1000).

**RESULTS:** Two types of nonenhancing lesions were identified; one with high signal intensity on fat-suppressed T2-weighted images (type A) and the other with low or intermediate intensity (type B). The type A nonenhancing lesions were observed in all the ameloblastomas, but they were evident in only 2 keratocystic odontogenic tumors. It is interesting to note that the ADCs of the nonenhancing lesions in the ameloblastomas were significantly higher than those of the nonenhancing lesions in the keratocystic odontogenic tumors ( $2.48 \pm 0.20 \times 10^{-3} \text{ mm}^2/\text{s}$  vs  $1.13 \pm 0.56 \times 10^{-3} \text{ mm}^2/\text{s}$ ;  $P < .001$ ). The ADCs of the solid lesions in the ameloblastomas ( $1.39 \pm 0.15 \times 10^{-3} \text{ mm}^2/\text{s}$ ) were significantly lower than those of the nonenhancing lesions in the ameloblastomas and were similar to those of the nonenhancing lesions in the keratocystic odontogenic tumors.

**CONCLUSION:** ADC determination may be used as an adjunct tool for differentiation between ameloblastomas and keratocystic odontogenic tumors.

**A**meloblastomas and keratocystic odontogenic tumors are major aggressive odontogenic tumors in the maxillomandibular regions. Both tumors display common radiologic features such as unicystic or multicystic lesions with extensive thinning and expansion of the overlying cortex. They are locally invasive and prone to recur after inappropriate surgical excision.<sup>1</sup> Furthermore, the effective preoperative differential diagnosis between these 2 tumors could help surgeons plan treatment because ameloblastomas require resection and keratocystic odontogenic tumors can be treated with enucleation.

Radiologic differentiation between these tumors is not difficult if the ameloblastoma is of the solid and multicystic type and the keratocystic odontogenic tumor is of the unilocular type. However, substantial ameloblastomas are unicystic, and some keratocystic odontogenic tumors are multicystic or multilobular with scalloped margins, thereby resembling ameloblastomas.

Several attempts have been investigated to differentiate between ameloblastomas and keratocystic odontogenic tumors with use of CT and MR imaging.<sup>2-5</sup> In this study, we further characterize these 2 aggressive benign tumors in the maxillomandibular regions on the basis of the diffusion-weighted MR imaging features, with particular emphasis on the apparent

diffusion coefficients (ADCs) of the nonenhancing lesions of these tumors.

## Materials and Methods

### Patients

We prospectively studied consecutive patients with ameloblastomas ( $n = 9$ ) or keratocystic odontogenic tumors ( $n = 7$ ) who received MR imaging examinations at our hospital from 2003 to 2006. The study protocol was accepted by the Ethics Committee of our hospital, and informed consent was obtained from each of these patients.

### Conventional MR Imaging

We performed MR imaging using a 1.5T MR scanner (Gyrosan Intera 1.5T Master; Philips Medical Systems, Best, the Netherlands) with a surface coil (11-cm Synergy Flex S or 4.7-cm microscopy coil; Philips Medical Systems). Axial and coronal T1-weighted images (TR, 500 ms; TE, 15 ms; numbers of signal intensity acquisition, 4 for S coil and TR, 550 ms; TE, 10 ms; numbers of signal intensity acquisition, 3 for microscopy coil) and axial fat-suppressed (spectral presaturation with inverted recovery [SPIR] or spectral-attenuated inversion recovery [SPAIR]) T2-weighted images (TR, 3741 ms; TE, 80 ms; numbers of signal intensity acquisition, 4 [SPIR] or TR, 5118 ms; TE, 80 ms; numbers of signal intensity acquisition, 4 [SPAIR] for S coil and TR, 3000 ms; TE, 90 ms; numbers of signal intensity acquisition, 6 for microscopy) were obtained for all the patients with use of a conventional spin-echo sequence and a turbo spin-echo sequence, respectively. The section thickness was 3 mm for the S coil and 2 mm for the microscopy coil. MR imaging was performed with a  $204 \times 256$  matrix for S coil and  $160 \times 128$  matrix for microscopy coil, a 18-cm FOV for

Received March 14, 2008; accepted after revision June 21.

From the Department of Radiology and Cancer Biology, Nagasaki University School of Dentistry, Nagasaki, Japan.

Please address correspondence to Dr. Takashi Nakamura, Professor and Chief, Department of Radiology and Cancer Biology, Nagasaki University School of Dentistry, Nagasaki, Japan; e-mail: taku@nagasaki-u.ac.jp

DOI 10.3174/ajnr.A1266

**Conventional MR imaging features of ameloblastomas and keratocystic odontogenic tumors**

MR Imaging Features	Ameloblastomas		Keratocystic Odontogenic Tumors
<i>n</i>	9		7
Maxilla/mandible	1/8		0/7
Size (L × S × H, cm), mean (± SD)	3.6 (1.2) × 2.3 (0.6) × 3.8 (0.9)		2.8 (0.5) × 1.4 (0.7) × 3.3 (1.2)
Tumor with solid wall	9		0
Signal intensity on T1/fsT2WI	Solid Lesion	Nonenhancing Lesion	Nonenhancing Lesion
Low/high	0	<b>7</b>	<b>1</b>
Intermediate/high	0	<b>2</b>	<b>1</b>
Low/intermediate	4	0	1
Intermediate/intermediate	5	0	4

**Note:**—T1/fsT2WI indicates T1/fat-suppressed T2-weighted images; L × S × H, average long axes (on axial T1WI) × short axes (on axial T1WI) × heights (on coronal T1WI). Solid and nonenhancing lesions indicate tumor areas with and without contrast enhancement, respectively. Bold figures indicate type A nonenhancing lesion with high-intensity signals on fsT2WI.

the S coil, a 7-cm FOV for the microscopy coil, and a 0.3-mm intersection gap for the S coil and 0.2 mm for the microscopy coil.

For the contrast-enhanced study, gadolinium was injected at a rate of 1.5 mL/s and at a dose of 0.1 mmol gadolinium/kg body weight. Enhanced and nonenhanced areas were referred to as solid and nonenhancing lesions, respectively.

On T1-weighted images, the signal intensity of a tumor was designated as high (signal intensity level similar to that of fat), low (similar to that of muscle), or intermediate (signal intensity level between that of fat and muscle); on fat-suppressed T2-weighted images, the signal intensity of a tumor was designated as high (similar to that of CSF), low (similar to that of muscle), or intermediate (intensity between that of CSF and muscle).<sup>4</sup>

**Diffusion-Weighted MR Imaging**

Diffusion-weighted axial images (TR, 4285 ms; TE, 87 ms; number of signal intensity acquisitions, 4) were obtained by the single-shot spin-

echo, echo-planar imaging technique with an FOV of 200-mm and matrix size of 112 × 90. The section thickness and section gap were 3 mm and 0.3 mm, respectively. We used the sensitivity encoding (SENSE) technique (SENSE factor, 2) to prevent susceptibility artifacts with a reduction in the echo-train length during the diffusion-weighted imaging. In some tumors, diffusion-weighted axial images (TR, 2973 ms; TE, 121 ms; number of signal intensity acquisitions, 6) were obtained with use of the microscopy coil. The section thickness was 2 mm. The diffusion-weighted MR imaging was performed with a matrix of 80 × 56, an FOV of 70 mm, and an intersection gap of 0.2 mm.

We determined the ADCs using 2 b factors (500 and 1000 s/mm<sup>2</sup>) and the following formula:

$$ADC = \ln(SI_1/SI_2)/(b_2 - b_1),$$

where *b*<sub>1</sub> (= 500 s/mm<sup>2</sup>) and *b*<sub>2</sub> (= 1000 s/mm<sup>2</sup>) are the gradient factors of sequences *S*<sub>1</sub> and *S*<sub>2</sub>, respectively, and *SI*<sub>1</sub> and *SI*<sub>2</sub> are the

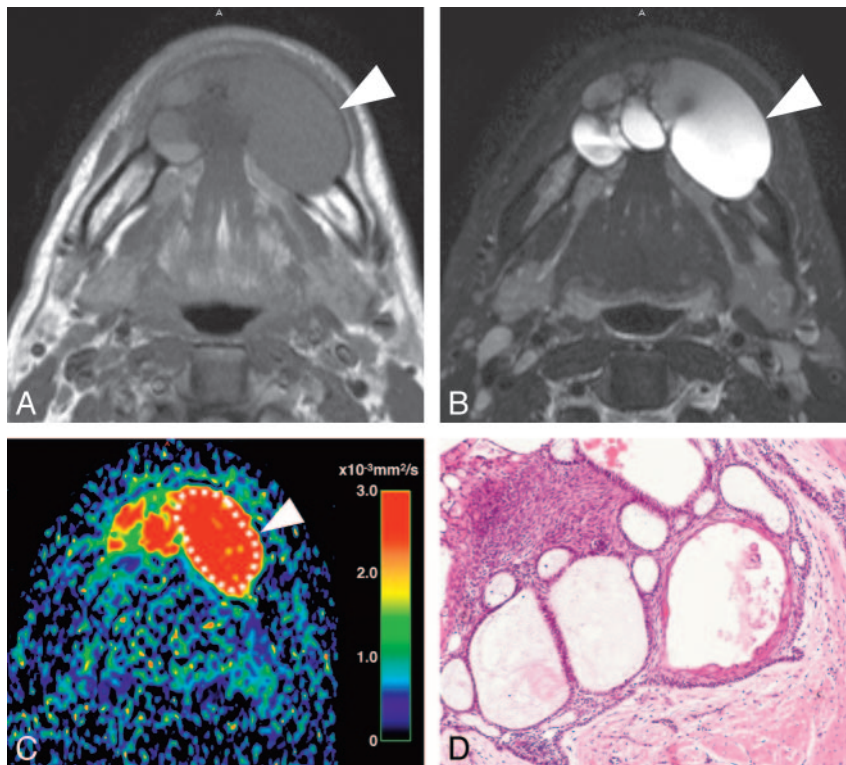


**Fig 1.** A 47-year-old man with ameloblastoma at the mandible. *A*, Axial T1-weighted image (TR, 500 ms; TE, 15 ms) shows the tumor (arrowhead) with low to intermediate signal intensity. *B*, Axial fat-suppressed (SPIR) T2-weighted image (TR, 3741 ms; TE, 80 ms) shows large, multiloculated cystic lesion with high signal intensity (arrowhead) indicative of cystic cavity. *C*, Axial color ADC map shows cystic tumor (arrowhead) with high ADC ( $2.50 \times 10^{-3} \text{ mm}^2/\text{s}$ ). Broken line indicates an irregular region of interest placed in the nonenhancing lesion. *D*, Photomicrograph shows solid tumor lesion associated with multiple small cysts, exhibiting a follicular pattern of tumor cell proliferation with peripheral palisading. Original magnification ×10.

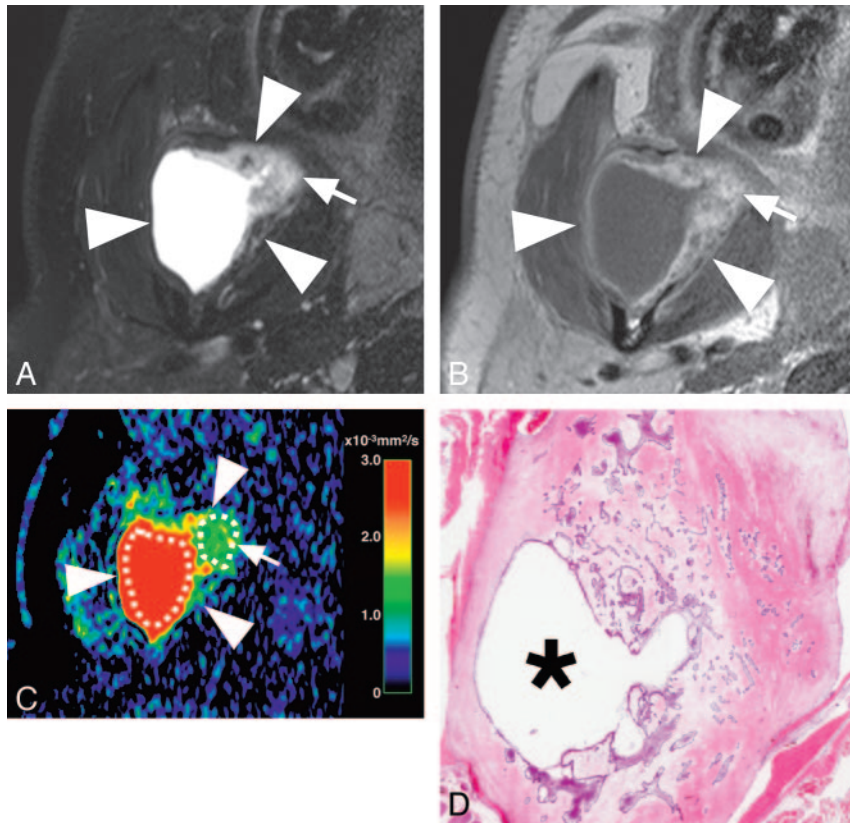


**Fig 2.** A 23-year-old man with ameloblastoma at the right mandible. *A*, Axial fat-suppressed (SPIR) T2-weighted image (TR, 3000 ms; TE, 90 ms) obtained by a 4.7-cm microscopy coil shows the tumor (arrowheads) with high signal intensity in the mandibular ramus. A solid lesion (arrow) is also observed. *B*, Axial contrast-enhanced T1-weighted image (TR, 550 ms; TE, 10 ms) shows the tumor (arrowheads) with clear definition between solid (arrow) and nonenhancing lesions. *C*, Axial color ADC map shows the tumor (arrowheads) consisted of nonenhancing lesion with high ADC ( $2.67 \times 10^{-3} \text{ mm}^2/\text{s}$ ) and a solid lesion (arrow) with intermediate ADC ( $1.50 \times 10^{-3} \text{ mm}^2/\text{s}$ ). Two broken lines indicate irregular regions of interest placed in solid (small) and nonenhancing (large) lesions. *D*, Photomicrograph shows large nonenhancing lesion (\*) associated with solid lesion containing follicular pattern of tumor cell proliferation with varying degrees of cystic degeneration in tumor islands. Original magnification  $\times 1$ .

signal intensities by sequences  $S_1$  and  $S_2$ , respectively. In general, when b factors greater than 300 are used, the resultant ADC contains negligible amounts, if any, of the perfusion factor. Therefore, we obtained ADC maps using the 2 abovementioned b factors. We obtained isotropic diffusion images by applying the 2 b factors along the 3 orthogonal directions. This procedure is more time-consuming; however, the simultaneous use of the SENSE technique can compensate for the excess time required. The total image acquisition time was 2 minutes 8 seconds per 25 sections with the SENSE technique. This rapid imaging allowed us to obtain ADC maps without significant motion artifacts.

In this study, we assessed ADCs of the nonenhancing and solid lesions within the tumors by averaging all of the ADCs determined on all the axial tumor images that contained the nonenhancing and solid areas. We calculated the ADCs by semiautomatically placing an irregular region of interest onto a nonenhancing or solid area; the region of interest was placed manually on a contrast-enhanced T1-weighted image so that it encompassed the entire area of the solid or nonenhancing lesions. Subsequently, the region of interest was automatically copied and pasted onto the corresponding ADC map.

### Image Analysis

We converted DICOM gray-scale ADC map images to color ADC map images using Photoshop 7.0 software (Adobe, San Jose, Calif), after setting the window level of the gray-scale ADC map images at  $1.5 \times 10^{-3} \text{ mm}^2/\text{s}$  and the window width at  $3.0 \times 10^{-3} \text{ mm}^2/\text{s}$  using

OsiriX software (<http://www.osirix-viewer.com>). As a result, tumor areas having high ADCs are displayed as color areas of shorter wavelengths such as red and tumor areas having low ADCs, as color areas of longer wavelengths such as blue. The conventional MR images and ADC maps correlated with the histologic findings of the excised tumors.

### Statistical Analysis

We assessed the significance of the differences in the ADCs between the 2 tumors by using Mann-Whitney  $U$  test with software (Version 13 for Windows; SPSS, Chicago, Ill).

### Results

#### Conventional MR Imaging

Contrast-enhanced MR imaging demonstrated that the ameloblastomas were composed of varying proportions of solid and nonenhancing lesions. However, the keratocystic odontogenic tumors exhibited thin, enhanced rims corresponding to the cyst walls. All of the ameloblastomas contained solid enhancing tissue, and none of the keratocystic odontogenic tumors exhibited such imaging features (Table). The nonenhancing lesions of the ameloblastomas and keratocystic odontogenic tumors exhibited low to intermediate signal intensities on T1-weighted images (Figs 1A and 2A; Table). On the other hand, the nonenhancing lesions were of low to



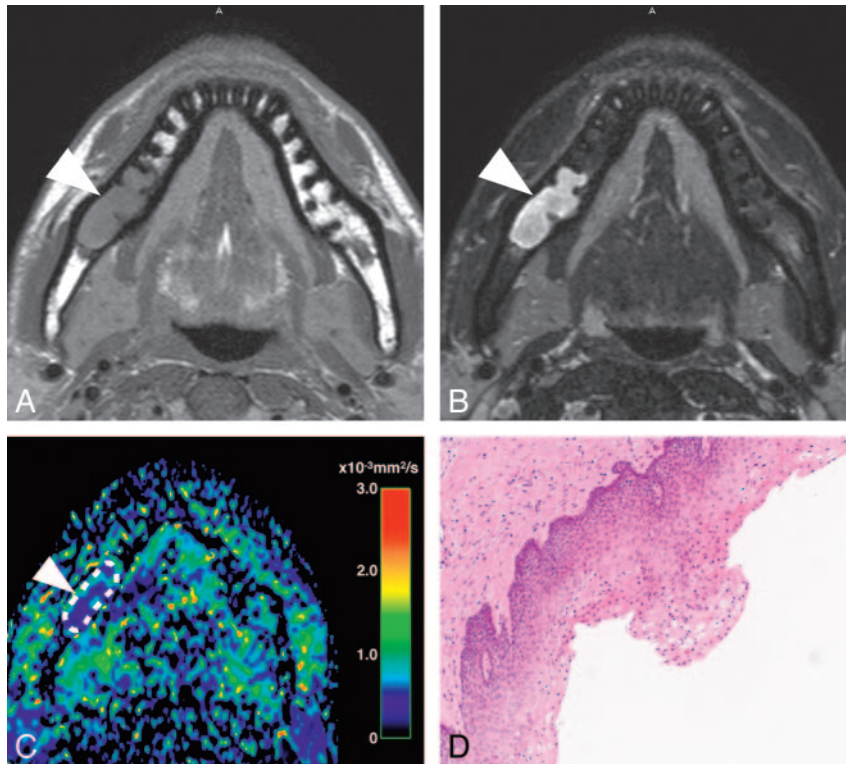


**Fig 3.** A 33-year-old man with a keratocystic odontogenic tumor at the right mandible. *A*, Axial T1-weighted image (TR, 500 ms; TE, 15 ms) shows a multilobulated cystic lesion with intermediate signal intensity (arrowhead). *B*, Axial fat-suppressed (SPAIR) T2-weighted image (TR, 5118 ms; TE, 80 ms) shows tumor (arrowhead) composed mainly of nonenhancing lesion with intermediate signal intensity. *C*, Axial color ADC map shows nonenhancing lesion (arrowhead) with low ADC ( $0.67 \times 10^{-3} \text{ mm}^2/\text{s}$ ). Broken line indicates an irregular region of interest placed in nonenhancing lesion. *D*, Photomicrograph shows cyst wall consisting of parakeratinized stratified squamous epithelium. Original magnification  $\times 10$ .

high signal intensity on fat-suppressed T2-weighted images (Figs 1*B* and 2*B*).

On the basis of the findings of the fat-suppressed T2-weighted images, 2 types of nonenhancing lesions were identified in the tumors: one with high signal intensity (type A) and the other with low to intermediate signal intensity (type B) (Table). The type A nonenhancing lesions were observed in all the ameloblastomas, but they were evident in only 2 cases of keratocystic odontogenic tumors. The solid lesions in the ameloblastomas were of intermediate signal intensity on fat-suppressed T2-weighted images (Table).

#### Diffusion-Weighted MR Imaging

The color ADC maps clearly delineated the nonenhancing and solid lesions of the ameloblastomas and keratocystic odontogenic tumors (Figs 1*C*, 1*D*, 2*C*, 2*D*, 3*C*, and 3*D*). Therefore, we compared the ADCs of the nonenhancing lesions in the ameloblastomas and keratocystic odontogenic tumors. The ADCs of the nonenhancing lesions in the ameloblastomas ( $2.48 \pm 0.20 \times 10^{-3} \text{ mm}^2/\text{s}$ ) were significantly higher ( $P < .001$ , Mann-Whitney *U* test) than those of the nonenhancing lesions in the keratocystic odontogenic tumors ( $1.13 \pm 0.56 \times 10^{-3} \text{ mm}^2/\text{s}$ ) (Fig 4).

When ADC of  $2.0 \times 10^{-3} \text{ mm}^2/\text{s}$  was used as a threshold for the differentiation between ameloblastomas and keratocystic odontogenic tumors, we obtained 100% sensitivity, 86% specificity, 94% accuracy, and 90% positive and 100% negative predictive values.

The ADCs of the solid lesions in the ameloblastomas ( $1.39 \pm 0.16 \times 10^{-3} \text{ mm}^2/\text{s}$ ) were significantly lower ( $P$

$< .001$ , Mann-Whitney *U* test) than those of the nonenhancing lesions in the ameloblastomas and were similar to those of the nonenhancing lesions in the keratocystic odontogenic tumors (Fig 4). The solid lesions of the keratocystic odontogenic tumors were so thin that precise ADC measurements were not achieved.

#### Discussion

Our study showed that ameloblastomas and keratocystic odontogenic tumors could be effectively differentiated on the basis of the ADC measurements of the nonenhancing lesions.

Diffusion seems to be influenced by “physical” parameters such as temperature, pressure, and viscosity. Furthermore, physiologic parameters can also influence diffusion; these are most significant because extracellular matrices and fluids are of great importance in the clinical context. The physiologic parameters include cellularity, amount and ratio of intracellular and extracellular water, nucleus-to-cytoplasm ratio, and vascularity. Significant changes in any of these parameters may result in changes in the pixel intensity of the diffusion-weighted sequence. If we use adequately high *b* values to eliminate signals from the vascular space (eg,  $b = 500$  and 1000), then the signal intensity would originate solely from intracellular and extracellular water.

Our finding that ADCs of the nonenhancing lesions differ significantly between the ameloblastomas and keratocystic odontogenic tumors indicates that the nonenhancing components vary between these 2 odontogenic tumors. Cystic spaces in the ameloblastomas usually contain slightly proteinaceous fluids, occasionally associated with colloidal materials.<sup>1,6</sup> The

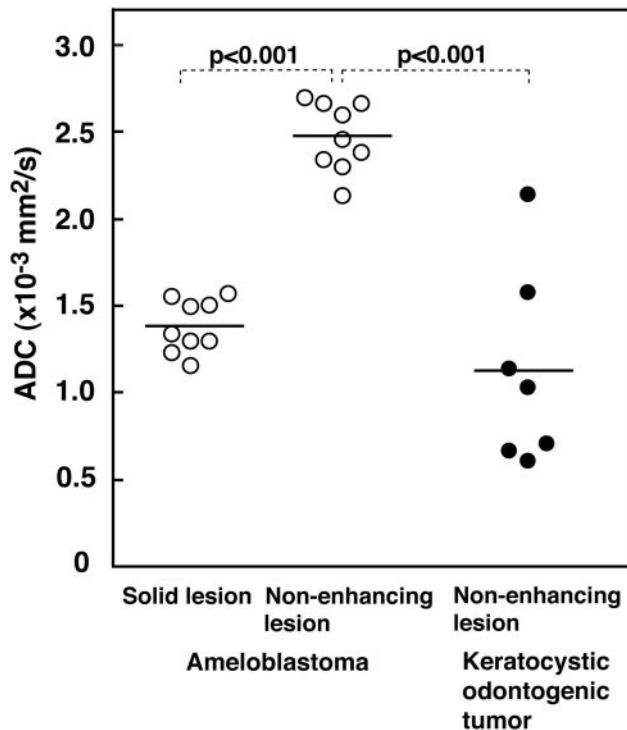


**Fig 4.** Scatterplot shows ADCs of nonenhancing and solid lesions of ameloblastomas and keratocystic odontogenic tumors. Horizontal lines indicate means of respective groups. *P*, Mann-Whitney *U* test.

cyst lumen of keratocystic odontogenic tumors often contains desquamated keratin.<sup>1,6</sup> This desquamated keratin accumulates in such large quantities that it influences the attenuations on CT images.<sup>7</sup> Therefore, it is plausible that such desquamated keratin increased the viscosity of fluids in the lumen, thereby decreasing the ADC levels of the nonenhancing lesions in keratocystic odontogenic tumors compared with those of ameloblastomas, in which increases in viscosity may be minimal.

Conventional MR imaging could also provide useful information about the differentiation of ameloblastomas and keratocystic odontogenic tumors.<sup>2,4</sup> In our study, we found that nonenhancing lesions were of high signal intensity on fat-suppressed T2-weighted images in all the ameloblastomas but in only 2 of the 7 keratocystic odontogenic tumors (Table). Therefore, the differentiation on the basis of T2-weighted images or T2 map would be useful. A previous study has reported that the cyst walls of the ameloblastomas were thicker than those of the keratocystic odontogenic tumors and were occasionally projecting into the cyst lumen; it is more interesting to note that the T2 relaxation time of the nonenhancing components was significantly shorter in the keratocystic odontogenic tumors than in the ameloblastomas.<sup>4</sup> The latter findings were consistent with our present results regarding the ADC measurement.

In the present study cohort, the discrimination of ameloblastomas from keratocystic odontogenic tumors on the basis of the presence of solid enhancing lesions was quite effective (Table). However, previous studies have shown that ameloblastomas exhibited a wide spectrum of T1-weighted and T2-weighted MR imaging features<sup>2,4</sup>; therefore, a significant over-

lap in the conventional MR imaging features may exist between ameloblastomas and keratocystic odontogenic tumors. A dynamic contrast-enhanced CT study showed a positive correlation between the enhancement ratio and microvessel attenuation in the ameloblastomas and keratocystic odontogenic tumors and further demonstrated that the enhancement ratios of the ameloblastomas were significantly higher than those of the keratocystic odontogenic tumors.<sup>5</sup> In the collective sense, these findings suggest that the discrimination of ameloblastomas from keratocystic odontogenic tumors on the basis of the ADC of nonenhancing lesions may be as effective as the differentiation between these tumors on the basis of contrast-enhanced study of solid lesions.

In addition to the ADCs of the ameloblastomas and keratocystic odontogenic tumors, we determined ADCs of the nonenhancing components of 6 dentigerous cysts; the ADCs of the dentigerous cysts were lower ( $1.56 \pm 0.78 \times 10^{-3} \text{ mm}^2/\text{s}$ ) than those of the ameloblastomas, though the difference was not significant because of broad SDs of the ADCs of the dentigerous cysts. The wide range of ADCs of the dentigerous cysts suggests that their nonenhancing components were considerably more heterogeneous than those of the ameloblastomas and keratocystic odontogenic tumors.

ADC measurement after placing volumetric regions of interest is time consuming. However, we found that ADCs of nonenhancing lesions in the 2 tumors were fairly uniform. Therefore, ADC measurement can be simplified by measuring ADC of a single representative nonenhancing lesion from each tumor.

## Conclusion

We demonstrated that ADCs of nonenhancing lesions in ameloblastomas were significantly higher than those of nonenhancing lesions in keratocystic odontogenic tumors. Although conventional MR imaging findings regarding the solid lesions in ameloblastomas were distinct from those in the case of keratocystic odontogenic tumors, the ADC measurement of the nonenhancing lesions may be useful as an adjunct tool for differentiation between these 2 locally aggressive tumors in the maxillo-mandibular region. The effective preoperative differential diagnosis between these 2 tumors would help surgeons plan treatment (resection or enucleation).

## References

- Harnsberger HR. *Diagnostic Imaging Head and Neck*. Salt Lake City: AMIRSYS; 2004
- Minami M, Kaneda T, Yamamoto H, et al. **Ameloblastoma in the maxillo-mandibular region: MR imaging**. *Radiology* 1992;184:389–93
- Han MH, Chang KH, Lee CH, et al. **Cystic expansile masses of the maxilla: differential diagnosis with CT and MR**. *AJNR Am J Neuroradiol* 1995;16:333–38
- Minami M, Kaneda T, Ozawa K, et al. **Cystic lesions of the maxillo-mandibular region: MR imaging distinction of odontogenic keratocysts and ameloblastomas from other cysts**. *AJR Am J Reontgenol* 1996;166:943–49
- Hayashi K, Tozaki M, Sugisaki M, et al. **Dynamic multislice helical CT of ameloblastoma and odontogenic keratocyst: correlation between contrast enhancement and angiogenesis**. *Comput Assist Tomogr* 2002;26:922–26
- Barnes L, Everson JW, Reichart P, et al. **Pathology and genetics of head and neck tumors**. In: *World Health Organization Classification of Tumours*. Lyon: IARC Press; 2005
- Yoshiura K, Higuchi Y, Arijii Y, et al. **Increased attenuation in odontogenic keratocysts with computed tomography: a new finding**. *Dentomaxillofac Radiol* 1994;23:138–42